



Characterisation of wave-influenced macroalgal propagule settlement

C.L. Stevens^{a,*}, D.I. Taylor^b, S. Delaux^{a,b}, M.J. Smith^a, D.R. Schiel^b

^a National Institute for Water and Atmospheric Research, PO Box 14-901 Kilbirnie, Wellington, New Zealand

^b School of Biological Sciences, University of Canterbury, New Zealand

Received 14 September 2006; received in revised form 5 November 2007; accepted 19 November 2007

Abstract

Successful attachment of macrophyte propagules in the rocky intertidal zone requires that propagules actually arrive at the substrate (settlement). The analysis first considers the small-scale processes occurring at the propagule scale then places these results in the context of long timescale variability in wave forcing due to weather and climate. The non-dimensional scaling is developed in terms of a Particle Reynolds number, Re_{sp} , that depends on both flow and particle scales. Scaling for size, inertia and buoyancy are described in terms of the Re_{sp} . Settlement mechanics of several macrophyte species (*Durvillaea antarctica*, *Hormosira banksii* and *Cystophora torulosa*) are compared using direct velocity measurements and placed in an environmental context using a twenty-year wave hindcast. The forcing is shown to be more closely linked to wave orbital speeds rather than breaker-driven phase speeds, and (negative) buoyancy has the greatest influence, identified through a Buoyancy Travel Ratio (BTR). Differences in these physical scales between the species are only moderate, suggesting supply, mucous and stickiness effects must be considered to fully resolve difference in success.

© 2007 Elsevier B.V. All rights reserved.

Keywords: Macroalgae; Propagules; Turbulence; Intertidal; Settlement; New Zealand; Fucooids

1. Introduction

Survival and propagation of macrophyte species in the rocky intertidal zone is one of the wonders of physical ecology. That plants have adapted to survive and thrive in such a harsh environment indicates the benefits of the ability to biomechanically evolve (Abelson and Denny, 1997). Survival under such conditions requires success at a number of stages including fertilization, arrival of the dispersive stage at the substrate (settlement), initial dynamical attachment and long-term stronger attachment (Clayton, 1992; Norton, 1992). These processes are little-understood for macroalgal species, particularly the arrival

stage that leads to settlement of propagules, which is the focus of this study.

In a single reproductive “event”, an individual adult intertidal fucoid alga may release many millions of fertilized propagules (see Schiel and Foster, 2006) into the water column often in a mucous matrix (Berndt et al., 2002; Schiel and Foster, 2006). However, the small size of propagules (~10–100 μm; Clayton 1992) means that their movement strongly follows that of the water within which they are held. While flow in the rocky intertidal is generally highly turbulent, the pathway to settlement must consider the flow very near the substrate. Seawater is viscous and so the relative velocity at all surfaces is zero. This “no-slip” condition, in conjunction with inherent fluid viscosity, results in a region close to surfaces where flow

* Corresponding author. Tel.: +64 4 386 0300.

E-mail address: c.stevens@niwa.cri.nz (C.L. Stevens).

variations are dampened and stress is transferred by molecular processes. As demonstrated here this viscous sublayer (VSL) can potentially be many times thicker than a propagule diameter. In the context of a stationary rocky substrate the passage of propagules across this sublayer is a key stage in the settlement process. Subsequent long-term attachment is studied elsewhere (Schiel et al., manuscript in prep.).

Boundary-layers in near-shore environments are complex and multi-scaled (e.g. Denny et al., 1992) but the essential mechanistic features are known (Grant and Madsen, 1986; Reidenbach et al., 2006) and from this the influence of the viscous sublayer on biology can be estimated (e.g. Gaylord et al., 2002; Koehl and Hadfield, 2004). However, the small scale and difficulty in directly observing behaviour at this scale has meant that ecological studies of propagules have tended to focus on larger scale processes. On the other hand ecological studies considering faunal species (e.g. Shimeta and Jumars, 1991; Eckman, 1996; Crimaldi et al., 2002) and transport of dissolved material have explicitly examined the role of the sublayer because it forms a direct link in any transport chain (e.g., Jorgensen and Revsbech, 1985; Dade, 1993; Baird and Atkinson, 1997; Hurd, 2000). The same consideration must be given to discrete propagules of marine algae. However, only a few studies of macrophyte propagule behaviour have been undertaken at these scales in the hydrodynamically complex intertidal zone (e.g. Gaylord, 1999).

To understand the structure of marine communities it is necessary to determine why a species is successful or not in particular situations. In New Zealand, for example, different species of fucoid algae dominate shores across gradients of wave exposure (Schiel, 2004). Massive *Durvillaea* spp. dominate the low intertidal region of high energy shores throughout much of the southern hemisphere, with *D. antarctica* found in southern New Zealand (Hay, 1994). The smaller fucoid *Hormosira banksii* characterises the mid-tidal zone of protected shores of New Zealand and southeastern Australia (Clarke and Womersley, 1981), and *Cystophora torulosa* is found lower on the shore in semi-protected areas (Schiel, 2004). Here we consider how the differing basic physical properties of propagules of these species impact on settlement processes in the VSL (Fig. 1). These properties and processes are fundamental to ecological dispersal and settlement dynamics of all such species (Table 1).

Of particular relevance to propagule settlement is the thickness of the VSL and its temporal persistence, because the propagule must cross this VSL to settle successfully (Abelson and Denny, 1997). Describing

propagule trajectories in the VSL requires consideration of microscale fluid mechanics (e.g. Burdick et al., 2001; Friedlander and Johnstone, 1957). Implicitly, at this scale viscosity dominates over inertia. A Reynolds number parameterization that combines flow with particle scale is encapsulated in the Particle Reynolds number Re_{*p} (Burdick et al., 2001) given as

$$Re_{*p} = \frac{u_* d_p}{\nu} \quad (1)$$

where u_* is the turbulent (friction) velocity scale, d_p is the length scale of an idealized propagule (here we chose equivalent diameter $d_p = \text{volume}^{1/3}$), and ν is the kinematic viscosity ($10^{-6} \text{ m}^2 \text{ s}^{-1}$). From this it is possible to identify the role of inertia in transporting propagules across the VSL. Clearly Re_{*p} is a property of the flow and the particle.

Other properties inherent in the particle, such as buoyancy, mucous coating and Brownian motion, may potentially contribute to settlement. This paper first develops scaling arguments associated with these processes. Beyond this, we hypothesize, variability in the background flow plays a dominant role that provides the opportunity, during extended periods of low energy,

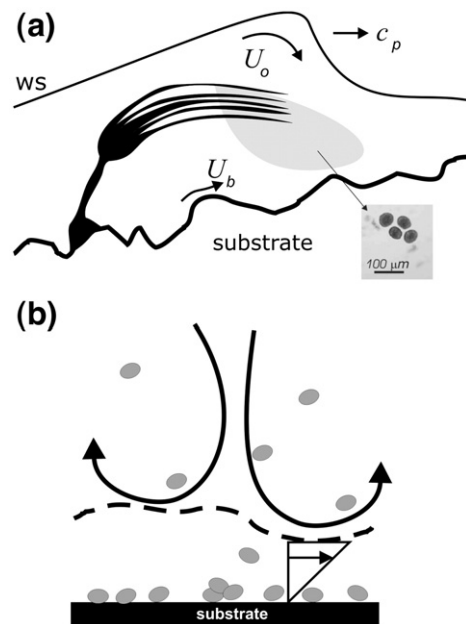


Fig. 1. (a) Sketch of macrophyte frond (*Durvillaea antarctica*) beneath the water surface (ws) with substrate and a pathway for released propagules (grey shading) to travel to the substrate, along with an inset of a propagule packet. Flow vectors relate to phase speed c_p , orbital motion U_o and near-bed flow U_b . (b) Sketch of the propagules in and around the (order 1 mm thick) viscous sublayer (denoted by dashed line), depicting shear flow in the VSL and eddies in the outer boundary-layer.

Table 1
Symbols, definitions and units

Symbol	Definition	units
a	Wave amplitude	m
$BTR = U_s T_p / \delta_v$	Buoyancy Travel Ratio (BTR)	–
C_d	Drag coefficient	–
c_p	Wave phase speed	$M s^{-1}$
D	Water depth	m
d_i	Inertial stopping distance	m
d_p	Particle diameter	m
D_p	Particle diffusivity	$m^2 s^{-1}$
f_p	Wave frequency	Hz
g	Gravitational acceleration	$M s^{-2}$
H_s	Significant wave height	m
$IDR = d_i / \delta_v$	Inertial Distance Ratio	–
$MDR = \frac{\rho_{pm} - \rho_0}{\rho_p - \rho_0}$	Mucous Density Ratio	–
$SR = d_p / \delta_v$	Scale Ratio	–
t_m	Time for mucous to dissolve	s
T_p	Wave period	s
u_*	Friction velocity	$m s^{-1}$
u'	Fluctuating horizontal velocity component	$M s^{-1}$
U_0	Orbital speed	$m s^{-1}$
U_s	Sinking speed	$M s^{-1}$
V_p, V_m	Volume of propagule and mucous	m^3
w'	Fluctuating vertical velocity component	$M s^{-1}$
δ_v	Viscous sublayer thickness	m
ν	Kinematic viscosity	$m^2 s^{-1}$
ρ_0	Seawater density	$Kg m^{-3}$
ρ_p	Propagule density	$Kg m^{-3}$
ρ_{pm}	Propagule mucous-modified density	$Kg m^{-3}$

for propagules to penetrate more deeply into the VSL and maximize their chance for surface-encounter. These arguments are then placed into the context of two sets of time and spatial scales: first, the propagule and viscous sublayer scales and second, the larger “outer scales” encompassing long-term variability of waves at weather and climate time scales. We use this approach to address several objectives which are as follows: (i) Determine the usefulness of the Particle Reynolds number in categorizing propagule settlement; (ii) Quantify the relative importance of size, inertia, Brownian motion and buoyancy in the context of settlement; (iii) Develop a framework for quantifying the role of biogenic mucous in influencing settlement; (iv) Determine if the settlement mechanics are affected by the outer “wave” scales and their variability; finally, (v) use the parameters to determine if between-species variability is important for settlement.

For reasons that will become clear in the Discussion, this study does not extend to include “attachment”, the next phase in the life-history of successful organisms in rocky systems after actual arrival. We start by describing the methods used to quantify physical forcing at the boundary-layer and observations at the “weather and climate” scales, then a scaling analysis describes the

basic processes in terms of non-dimensional parameters. In the Results section the scaling is explored using the observations. The Discussion compares the relative importance of the various processes involved in settlement and the implications for between-species variations in properties.

2. Methods

2.1. Propagule properties

Three physical properties of propagules: diameter, density and sinking rate in seawater, were measured for the three fucoid species, *Durvillaea antarctica*, *H. banksii* and *C. torulosa*. Taylor and Schiel (2003) and Schiel (2006) provide an ecological context for these three species. Another important property is the nature of the mucous coating that can surround propagules. While this coating may sometimes be only a few microns thick (Clayton, 1992), it can also form a material matrix that substantially increases the “size” of the propagule. Diameters were measured on live propagules which were collected in seawater from reproductive adults within 15 min of release. Sinking rates of an injection of many propagules were measured by placing propagules in a 700 mm high vertical column of seawater of known density and temperature, and using particle-tracking software (Fluidstream, Nokes, 2005). Densities were calculated using Stokesian mechanics (see Section 3.3) for spherical bodies (Coon et al., 1972; Taylor et al., 2008), whereby density is inferred from radius, sinking rate and seawater properties. The averages of three replicate trials were used. The variability is discussed elsewhere (Taylor et al., 2008).

2.2. Wave-driven boundary-layer measurements

Wave velocity, surface elevation and pressure data were recorded on a rocky reef platform at Kaikoura, New Zealand (Fig. 2; latitude 42.417S; longitude 173.715E), near the Edward Percival Field Station operated by The University of Canterbury. Hence, there is a reasonable understanding of many aspects of the local intertidal/subtidal ecology (e.g. Chiswell and Schiel, 2001; Taylor and Schiel, 2003; Dunmore and Schiel, 2003, Schiel, 2004, 2006). The majority of published rocky-shore turbulence data come from subtidal sites (except e.g. Gaylord, 1999). For our study we worked on the outer edge of the reef platform, which is around 250 m wide. Water depths on the platform reached 1.5 m at high tide. Depths 300 m offshore of the platform edge were around

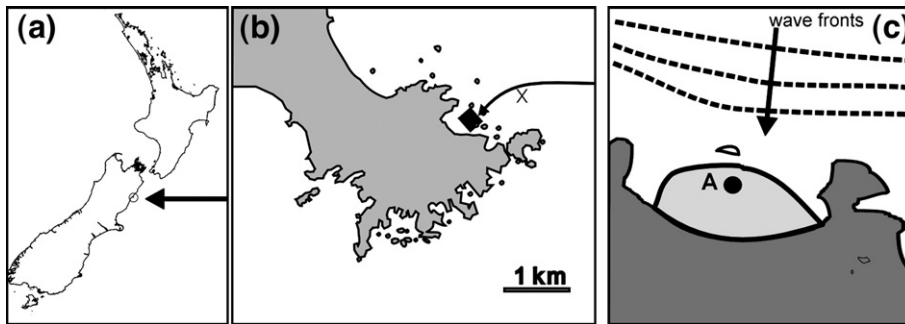


Fig. 2. Field site showing (a) the location of Kaikoura Peninsula on the South Island of New Zealand, (b) the peninsula itself (X marks the wave rider) and (c) the field site with the shore region (dark grey) showing the reef (light grey), the incoming wave fronts and the location of the velocity sensor A.

12–15 m which slowly deepened to 25 m a km further offshore. An in-house built wire-wave gauge was placed next to a Nortek-AS Vector on a sturdy frame. The Vector sensor head was placed facing downwards on the offshore side of the frame in such a way that the sensor volume was (5 cm) above the bed at a location where the average water depth went from 0 to 1.5 m. These near-bed velocity and pressure data were recorded for a total of 100 h over five days, at 16 Hz, using a sample volume of around 1 cm³ in 19,200 data-point bursts (20 min). Estimation of spectral properties used a range of segment sizes, depending on the trade-off between confidence and inclusion of low frequency bins. All spectral segments were pre-filtered with a Hanning window (Emery and Thomson, 1997). The Vector velocimeter has higher signal-to-noise capabilities in the vertical (w) than in other directions and so its turbulence spectrum is of higher quality. The friction velocity u_* can be determined, assuming the velocimeter is in the constant stress layer, using the Reynolds Stress covariance argument $u_* = (-\overline{u'w'})^{1/2}$ where the prime denotes perturbation from the mean of horizontal (u) and vertical (w) velocity component timeseries and the overbar represents an averaging (Kim et al., 2000).

2.3. Offshore waves and the wave hindcast

A Datawell waverider buoy was located offshore, providing standard wave parameters (Fig. 2) for a month-long period during the field campaign. A long-time context was provided using a 20-year wave hindcast (Gorman et al., 2003) which provided wave climate data offshore of the field site (Fig. 2b). The hindcast model was driven by European Centre for Medium Range Weather Forecasting re-analysis wind-fields, and run on a 1.125 × 1.125 degree grid for the SW Pacific and Southern Ocean region. Directional spectra, saved at grid cells around the coast, were

interpolated to points on the 50 m isobath and filtered to account for limited fetch to the coastline (Gorman et al., 2003). The hindcast generates 3-hourly estimates of significant wave height H_s and the frequency of the peak of the wave spectrum f_p (represented in the following by period $T_p = 1/f_p$). The shallow water wave model SWAN was then used to propagate the wave energy inshore to the 10 m contour (Gorman et al., 2003).

3. Non-dimensional scaling analysis

Understanding propagule–VSL interactions requires comparison of the relative importance of a variety of properties and processes. Here we consider non-dimensional scaling of the imposed physical processes such as waves and turbulence as well as “biological” properties like buoyancy.

3.1. Wave forcing

The rocky intertidal/subtidal zone is an energetic fluid environment. While the majority of energy is contained in the tides, shoaling ocean waves have a direct and significant impact on the shoreline. Wave development and motion is multi-faceted especially near shore (e.g. Young, 1999). There are three relevant wave “speeds”, (1) the water particles move in orbital paths at the “orbital speed”, (2) wave crests move at the “phase speed” and (3) the energy contained in the wave field moves at its own “group velocity”. In deep water the energy travels at half the phase speed and the wave frequency controls the speed of wave propagation. However, once waves reach shallow water ($< \text{wavelength}/20$) the water depth, d , and wave amplitude, a , largely control behaviour, and the onset of wave breaking and the phase speed and group velocity are equal.

For shallow water waves, the oscillatory orbital flow speed U_o at location x and time t is given by (e.g. Young, 1999)

$$U_o = a \left(\frac{g}{d} \right)^{0.5} \sin(\psi) \quad (2)$$

where a is the wave amplitude (i.e., $H_s/2$), g is gravitational acceleration, d is water depth and $\psi = kx - \omega t$ is the location in wave-number ($k = 2\pi/\text{wavelength}$)–frequency (ω) space. The shallow water phase speed is given by $c_p = (gd)^{1/2}$. Near-bed velocities are driven by the wave orbital speed. However, at the point just after wave breaking, the plunging “breaker” moves at a speed comparable to the phase speed of the wave and one might expect actual speeds to vary between c_p and U_o . Numerically, for $a = 1.0$ m and $d = 2.0$ m, $U_o = 2.2$ m s⁻¹ while $c_p = 4.4$ m s⁻¹. Observations of these velocities are compared with scaling in the Results section.

3.2. The boundary-layer

The wave-induced flow above the substrate results in a periodically-forced turbulent boundary-layer and, adjacent to the surface, a concurrently varying VSL. The degree of turbulence in the boundary-layer is affected by the “roughness” of the substrate. The engineering literature describing flow over surfaces represents the stress transfer using a drag coefficient C_d based on whether or not the substrate roughness length scale is small relative to the VSL thickness δ_v , as well as flow speed (e.g. Schlichting, 1979). The friction velocity scale, u_* , associated with the turbulence in the boundary-layer, enables estimation of the VSL thickness, $\delta_v = 5\nu/u_*$ (e.g. Tritton, 1988) where $u_* = (C_d)^{1/2} U_o$. Feddersen et al. (2003) demonstrated the complexity of C_d and that it was likely also linked to wave breaking and not solely correlated with bottom roughness. Reidenbach et al. (2006) find $C_d = 0.009 - 0.015$ for flow over coral reefs. For present purposes it is specified as $C_d = 0.01$ (e.g. Puleo and Holland, 2001) and this is discussed later. Substituting for u_* in Eq. (1) enables the Re_{*p} to be related to the wave environment as

$$Re_{*p} = \frac{H_s}{2} \left(C_d \frac{g}{d} \right)^{1/2} \frac{d_p}{\nu} \quad (3)$$

A comparison of particle size to viscous sublayer thickness results in a “Scale Ratio” SR given by

$$SR = \frac{d_p}{\delta_v} = \frac{1}{5} Re_{*p} \quad (4)$$

This ratio allows a direct comparison of the propagule scale with the thickness of the viscously domi-

nated region. If the propagule diameter is very small relative to the δ_v ($SR \ll 1$) then settlement will rely heavily on molecular processes.

3.3. Buoyancy effects

A priori the second-most important propagule scale, after size, is its settling speed in a quiescent fluid due to the (negative) buoyancy of the propagule. Because the physical scale is relatively small and the shape is relatively spherical (Clayton, 1992) we can assume, in the first instance, a Stokesian buoyancy-induced propagule settling speed U_s so that

$$U_s = \frac{2}{9} \frac{(d_p/2)^2}{\nu} g' \quad (5)$$

with $g' = g(\rho_p - \rho_0)/\rho_0$ defining a modified gravity (ρ_p and ρ_0 are the propagule and background fluid densities respectively and g is gravitational acceleration). The distance a particle travels due to buoyancy within a wave period, relative to δ_v , is then encapsulated in the Buoyancy Travel Ratio (BTR) given as

$$BTR = \frac{U_s T_p}{\delta_v} = \frac{1}{90} (Re_{*p})^2 \left(\frac{g' T_p}{u_*} \right) \quad (6)$$

The right-hand most term in brackets is the ratio of the buoyancy-induced velocity within a wave period to the turbulent velocity scale. The overall distance comparison scales with the $(Re_{*p})^2$ but with other dependencies.

3.4. Inertia

A propagule can potentially cross the VSL purely due to the initial momentum imparted outside the VSL. This is quantified using the “stopping distance” (e.g. Friedlander and Johnstone, 1957)

$$d_i = \frac{u_* \rho_p d_p^2}{18 \rho_0 \nu} \quad (7)$$

Hence, the ratio of d_i to δ_v described here as the Inertial Distance Ratio can be cast in terms of Re_{*p} so that

$$IDR = \frac{d_i}{\delta_v} = \frac{1}{90} Re_{*p}^2 \quad (8)$$

3.5. Brownian motion

At this micro-fluidic scale, Brownian motion, inherent random motion due to internal molecular-

level thermal fluctuations, may be important. It is represented by a particle Diffusivity D_p (e.g. Shimeta, 1993) given by $D_p = KT/(3\pi T_0 v d_p)$ where K is Boltzmann's constant ($1.38 \times 10^{-23} \text{ m}^2 \text{ kg s}^{-2} \text{ K}^{-1}$) and T is temperature in degrees Kelvin. Generically a diffusive lengthscale scales as the square root of the product of the diffusivity and time. Thus, a comparison of lengthscales in the manner of Eqs. (4), (6) and (8) is $(Sc)^{1/2}$ where the Schmidt number $Sc = \nu/D_p$ compares a given diffusivity to molecular diffusion of momentum (i.e. ν).

4. Results

4.1. Propagule properties

The average properties measured in laboratory experiments are shown in Table 2.

4.2. The wave field

The waves from the peak of the wave spectrum at the field site are predominantly around 10 s in period or less (Fig. 3a). Clearly, the largest waves in terms of height usually have the longest wavelength (Fig. 3b). In addition nearly 1% of waves are 3 m or greater in significant wave height (Fig. 3c). All but the shortest wavelength waves are significantly attenuated by the time they reach the shore, but this will be location-dependent. At the Kaikoura field site (Fig. 2b) there was approximately a factor of 2.5 reduction in amplitude from deep water (as measured by the wave buoy, Fig. 2) into the reef system (Fig. 4). As the hindcast has propagated the waves into 10 m (i.e. shallower than the wave buoy) it is assumed these hindcast amplitudes are reduced by a factor of two by the time they reach the sample site. While approximate, this is suitable for scaling. The hindcast timeseries of H_s then allows climatological distributions of wave phase and orbital speed to be determined.

4.3. The turbulent boundary-layer

In order to combine these hindcast data with other properties to estimate SR, IDR and BTR, the connection

Table 2
Propagule average properties

	Diameter μm	Density kg m^{-3}	Sinking rate mm s^{-1}
<i>Durvillaea antarctica</i>	29	1780	0.36
<i>Hormosira banksii</i>	61	1330	0.67
<i>Cystophora torulosa</i>	100	1190	0.89

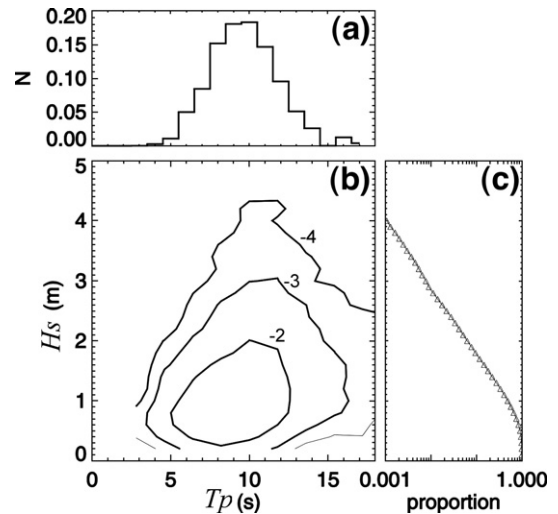


Fig. 3. Significant height vs period of spectral peak distribution from a twenty-year wave hindcast at the 10 m contour off-shore of the Kaikoura Peninsula as marked in Fig. 2b. (a) A histogram of T_p , (b) contours in \log_{10} units of proportional realization and (c) the cumulative H_s distribution. So in (b) the situation where $T_p=10$ s and $H_s=2.0$ m occurred 10 times more often than that where $T_p=10$ s and $H_s=3.0$ m.

between u_* and the waves needs to be described. Section 2 assumed u_* was controlled by wave orbital velocities and a fixed drag coefficient. Simultaneous velocity and pressure measurements from the Vector velocimeter enable velocity scale estimates for the phase speed and orbital speed, as well as the direct near-substrate velocity measurement required to determine $u_* = (-\overline{u'w'})^{1/2}$. The direct comparison of velocity scales (Fig. 5) shows orbital speeds are closer to a speed inferred from u_* (i.e. $U_b = (-\overline{u'w'})^{1/2}/(C_d)^{1/2}$) than the phase speed. While this can potentially vary with degree of wave breaking, the water was reasonably shallow during these observations and breakers were regularly observed at the sample point.

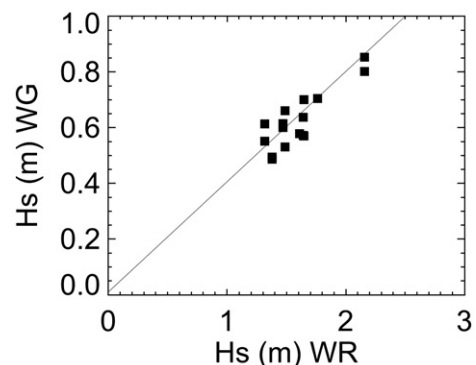


Fig. 4. Comparison of waverider-derived H_s (H_s WR) at the offshore station with inshore measurements right on the reef at the wave gauge (H_s WG). The line has a slope of 1/2.5.

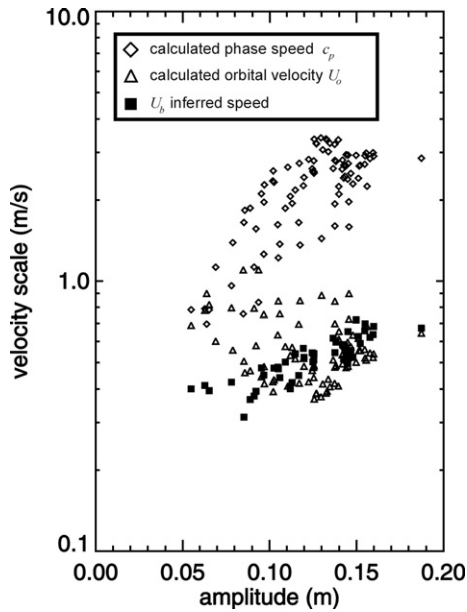


Fig. 5. Velocity scales as a function of wave amplitude as determined by standard deviation of water depth. The velocity scales include calculated phase speed (c_p), calculated orbital velocity maximum (U_o) and a u_{*i} inferred from the measured Reynolds stress as described in the text.

Furthermore, while the wave amplitudes of Fig. 5 appear small it should be recalled that their offshore equivalents are around 2.5 times larger and so represent a common range of wave forcing (Fig. 3). The main implication of Fig. 5 is that we can proceed using a U_o -based connection between u_* and the hindcast wave field.

It is useful to consider the problem from the perspective of the frequency domain as it enables, to some degree, a separation of waves from both slower and faster processes. Spectral analysis of high-frequency time series of velocity and pressure data recorded with the acoustic velocimeter illustrates the flow variability (Fig. 6) and potentially allows “direct” estimation of u_* using inertial dissipation (Kim et al., 2000; Reidenbach et al., 2006). At the lowest frequencies (perhaps periods of 50–100 s, i.e. $f < B$, Fig. 6) slow changes in currents and water depth driven by variability in near-shore currents, as well wave-group effects maintain energy at low frequencies (c.f. McGregor et al., 1998). An equilibrium wave spectrum (slope falls off as f^{-4}), whereby wind energy is fed in at the same rate as it cascades to smaller scales, is weakly apparent at frequencies between the peak of the spectrum (0.08 Hz) and around 0.13 Hz.

The horizontal velocity spectrum $S(U)$ shows the influence of the waves more strongly than the vertical

velocity spectrum $S(W)$ because the waves in shallow water have an elliptical motion which results in a stronger horizontal signal. The frequency range 0.15–0.6 Hz sustains a shoulder region, possibly due to local turbulent kinetic energy production. By 1.0 Hz there is a constant slope region, close to $f^{-5/3}$ at least for W . The local peak in the pressure at 5 Hz (A in Fig. 6) is most likely some kind of flow-induced vibration so that the spectra should be ignored at this, and higher, frequencies. However, these spectra are nowhere near as “clean” as those shown in Kim et al. (2000) and Reidenbach et al. (2006), so the comparison of Reynolds stress-derived u_* as justification for the use of U_o will be maintained for the purposes of estimating IDR, SR and BTR.

4.4. The Particle Reynolds number

The Re_{*p} controls the SR and IDR, and strongly influences the BTR. The length scale d_p only varies over an order of magnitude in the range $d_p = 20\text{--}200\ \mu\text{m}$, where the larger scale is for an aggregate of propagules. The near-bed velocity (assumed equivalent to U_o) varies over perhaps two orders of magnitude ($0.01\text{--}1.0\ \text{m s}^{-1}$) so that $u_* = 1 \times 10^{-3}\text{--}0.1\ \text{m s}^{-1}$. Hence Re_{*p} will range

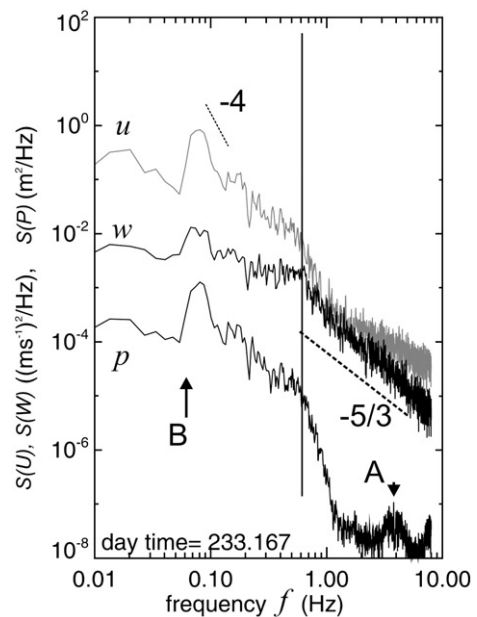


Fig. 6. Spectral analysis of two components of velocity (w = vertical; u = horizontal) and pressure p . The pressure data have been offset downwards by two orders of magnitude. Marked lines show slopes of $f^{-5/3}$ and f^{-4} for reference. The vibration effect discussed in the text is identified with arrow A. The “expected” low frequency roll-off is marked by arrow B.

Table 3
Non-dimensional scaling parameter range summary

Parameter	Form	Explanation	Range
Particle Reynolds number Re_{*p}	$Re_{*p} = \frac{u_* d_p}{\nu}$	$Re_{*p} \gg 1$, highly energetic flow relative to scale of propagule (but the VSL may still be important).	0.02–20
Scale Ratio SR	$SR = d_p / \delta_v$	$SR > 1$, propagule is much larger than VSL thickness so even small perturbations in particle position mean it may encounter surface. $SR < 1$ propagule significantly influenced by molecular-scale processes.	0.004–4
Buoyancy Travel Ratio BTR	$BTR = U_s T_p / \delta_v$	$BTR > 1$, propagule can rapidly traverse VSL due to buoyancy before next wave “compresses” the VSL.	$2 - 1 \times 10^4$ (no mucous)
Inertial Distance Ratio IDR	$IDR = d_i / \delta_v$	$IDR > 1$, turbulence outside VSL is sufficient to “shoot” propagules directly across VSL into substrate.	$4.4 \times 10^{-6} - 4.4$
Mucous Density Ratio MDR	$MDR = \frac{\rho_{bm} - \rho_0}{\rho_p - \rho_0}$	$MDR < 0$, mucous is sufficient to make propagule float. $ MDR \gg 1$ then mucous dominates overall buoyancy.	Unknown

over three orders of magnitude between 0.02 and 20. This enables estimation of SR, IDR, BTR and Sc .

Given this range of Re_{*p} , then the $SR = 0.004 - 4$, indicating that only in extreme circumstances will the VSL thickness be comparable or thinner than the diameter of the propagule. Therefore, almost all propagules will have to cross the molecular-diffusion dominated VSL. Consideration of inertia-driven crossing of the VSL using the IDR indicates a span of $IDR = 4 \times 10^{-6} - 4$. This suggests it is possible that under more energetic conditions propagules can be directly “shot” across the VSL, reaching the wall before viscosity slows them. Similarly, the BTR ranges over $2 - 10^4$. The Schmidt number Sc due to Brownian motion evaluates to around 10^9 due to the very low diffusivity, so Brownian motion can be rejected as playing a dominant role in arrival. Table 3 summarizes the scaling results.

5. Discussion

The scaling enables the construction of a process-oriented picture of the drivers of initial contact for macrophyte propagules using both field observations of hydrodynamics and laboratory measurements of propagule properties to provide a context. The following considers each of the objectives posed in the introduction.

5.1. Parameterizing propagule settlement using the Particle Reynolds number

The parameter is clearly fundamental in the scaling for inertia, size and buoyancy effects (although Re_{*p} is not the sole parameter in the latter). Furthermore, typical values span unity, suggesting that a significant difference in behaviour is possible depending on the fluid–propagule situation. This does allow some focusing of analysis of sensitivity to various parameters. For example, the pre-

sence of a macroalgal canopy will likely affect the local C_d but we believe the substrate variability and the large scale — comparable to wavelength (~ 50 m) is probably just as important. The contribution of bedform drag is the biggest effect not being captured — i.e., what is the effect of all the lumps and bumps in the reef platform structure, not to mention the face of the platform itself.

5.2. The relative importance of scale, inertia, Brownian motion and buoyancy

The scaling uses δ_v as the delineation between the viscously dominated region adjacent the substrate and the turbulent water away from the surface. It is important to reiterate that the thickness δ_v defines no real material interface in the fluid. It represents the scale at which viscous forces are equivalent to inertial forces and this will be subject to temporal considerations. Consequently, it is possible for the artificial line marked by the constantly varying δ_v to pass by a propagule as U_b changes, thus “moving” the propagule from the laminar to the turbulent regime or vice versa.

The relative importance of scale, buoyancy and inertia (and ignoring Brownian motion because of the small Sc) can be considered as a function of Re_{*p} (Fig. 7). If we first consider the relative importance of scale (SR) and inertia (IDR) in the absence of any buoyancy influence, Fig. 7 suggests that at any given Re_{*p} , and with all other things being equal, the settlement will be dominated by the scale effect. The inertial effect will only exceed the scale effect beyond the level at which settlement will have already occurred. Consequently, the inertial effect might be considered a perturbation on the scale effect.

However, if there is a density difference, as is clearly the case from the sinking tube measurements, then buoyancy has the potential to dominate the settlement process. Fig. 7 shows that even a moderate density perturbation is

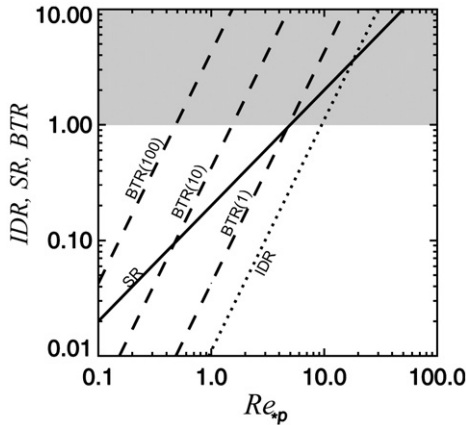


Fig. 7. IDR; SR and BTR etc as functions of Re_{sp} . The solid line is SR, the dotted line is IDR and the dashed lines are the BTR for three different buoyancies of propagule (density perturbations $\Delta\rho=1, 10, 100 \text{ kg m}^{-3}$ respectively). The shaded region is where the scale associated with the particular mechanical process is greater than the VSL thickness.

sufficient to exceed the effect of the thinning VSL with BTR's >10 very likely. The influence, from the perspective of an increasing Re_{sp} will be felt before that due to inertia and scale. An order of magnitude variability in the propagule density perturbation is sufficient to shift the effect of buoyancy from being negligible (i.e. SR and IDR both >1 before BTR) through dominating the process (Fig. 7). Thus, it appears buoyancy has a significant role to play despite the initial impression that the significant energy in the intertidal zone would tend to overcome buoyancy. Once the propagule is in the VSL, buoyancy and high background flow speeds (i.e. small δ_v) work in concert. Essentially buoyancy-driven motion is substantial within a wave period given the small distances (δ_v) to cross.

5.3. Quantifying the mucous effect

The BTR suggests buoyancy dominates the entire process of crossing the VSL. However, while the propagules are themselves negatively buoyant, upon release they are encased in a mucous of density ρ_m which increases the scale, and with the mucous generally being less dense than seawater, changes the buoyancy of the propagule packet. Keeping with the spherical assumption, the mucous increases the radius by r_m so that the final propagule diameter is $d_p + 2r_m$. The propagules are negatively buoyant ($\rho_p > \rho_0$) but the mucous is positively buoyant ($\rho_m < \rho_0$) so that the overall density is given by the volumetric average

$$\rho_{pm} = \frac{V_p \rho_p + V_m \rho_m}{V_p + V_m} \tag{9}$$

where mucous volume is $V_m = r_m^3 + (3d_p/2)r_m^2 + (3d_p^2/4)r_m$. Hence, ρ_{pm} should replace ρ_p in the g' estimate. A Mucous Density Ratio $MDR = (\rho_{pm} - \rho_0) / (\rho_p - \rho_0)$ is one way of parameterizing the effect of the mucous. The denominator is always positive based on present evidence while the numerator could be either sign. The magnitude of the MDR indicates the relative effect of the mucous.

An additional factor is the temporal dimension of the mucous, including the time for mucous to dissolve, t_m , which effectively results in buoyancy-induced motion changing sign. How coherent is the propagule package and its mucous coating? If they remain coherent for a significant period then propagule packages could rise upwards through the VSL on overhanging walls. If the propagules are not well-bonded to the mucous, they might rapidly “sink out” of the mucous and it will have no further influence on settlement. At this stage, because of this temporal variability, there are no data available to reliably estimate the proposed MDR parameter but the sensitivity to buoyancy described above suggests it should be a future research priority.

5.4. The effect of the outer “wave” scales and their variability

The SR and IDR are entirely related to near-bed speeds, which are controlled by wave height in shallow water. However, the buoyancy effect relates to wave period also. The distribution of BTR for a given species (Fig. 8) shows how BTR is always greater than 1 in the

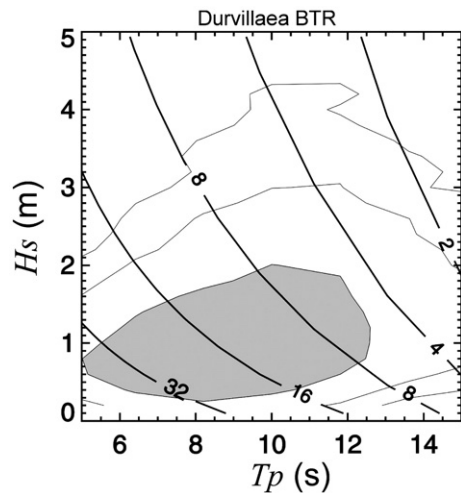


Fig. 8. Nearshore BTR for *Durvillaea antarctica* as a function of the driving 10 m contour wave conditions H_s and T_p and superimposed on the offshore wave distribution described in Fig. 3 with the most common wave domain shaded. The wave attenuation has been included in the BTR calculation.

region of most waves. Because of the form of (7) the BTR should ideally vary at the wave frequency. Hence, the wave parameters set the magnitude and frequency of the boundary-layer development. In addition, a typical ocean wave-field supports a spectrum of wave energy whereby waves exist in packets or groups. While on average $a \sim H_s/2$, instantaneously a varies at the frequency of the wave packet amplitude. It is likely that a more complex representation than a simple fixed wave period and wavelength is required to understand settlement. One of the key parameters in determining the path a propagule takes as it moves within the VSL is the return period before the next wave of a magnitude large enough to reduce the VSL to the location of the propagule, thus returning it to the turbulent boundary-layer. Consequently, it is the time between extremes that is important and more specifically the time between a fast flow and the next fast flow of a greater magnitude.

The timing of such events can be viewed through a form of return-period analysis akin to the lull-time de-

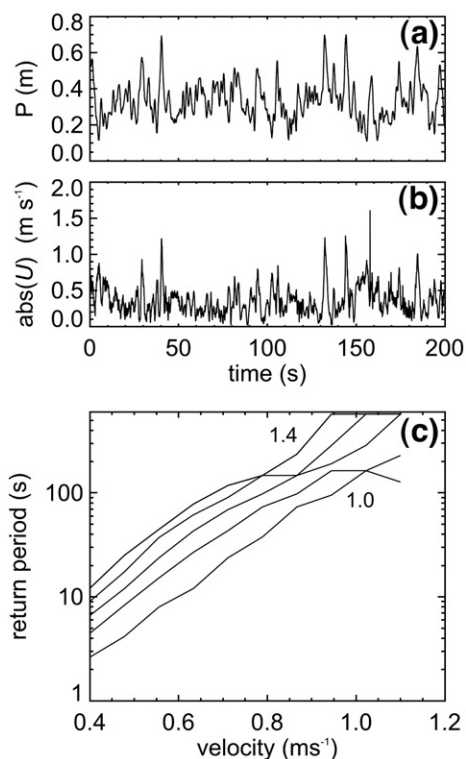


Fig. 9. Return period of faster velocity events. Sections of time series of (a) pressure (water depth), and (b) near-bed velocity. (c) Isolines of the average return period of a proportionally greater velocity event, as a function of the initial velocity event. For example, an event that reaches $0.8 m s^{-1}$ takes, on average, 40 s for the velocity to return to $0.8 m s^{-1}$, and around 150 s for the velocity to reach $1.4 * 0.8 m s^{-1}$. The higher values are biased as the data record is only 1200 s long.

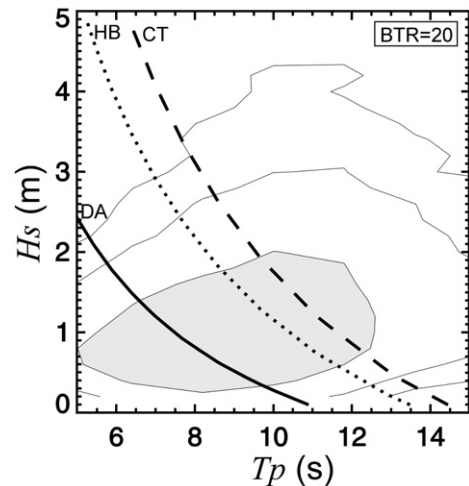


Fig. 10. BTR=20 contours for three different species (*Durvillaea antarctica* — solid; *Hormosira banksii* — dotted; *Cystophora torulosa* — dashed) overlaid on the driving 10 m depth wave distributions of Fig. 3, with the shading indicating the 10 most common waves. The wave attenuation has been included in the BTR calculation.

veloped by Crimaldi et al. (2002) except here we are interested in return periods of faster events. The same time series used in Fig. 6, now plotted explicitly in Fig. 9a, has a large spike at $t=40$ s, then some 90 s later three reasonable-sized events occurred over a 50 s period. This variability is smoothed out over the full timeseries (6 times longer than the plotted sub-section). An analysis of scaled return periods (Fig. 9b) indicates a great deal of sensitivity to velocity increase. The return period of a velocity event 40% larger results in around a ten-fold increase in return period.

The hypothesis is that the large events compress the VSL and then, if followed by a lull, this provides the best conditions for propagule settlement. This is supported by the fact that waves are clearly far from constant or even linear in the intertidal. It does result in the velocity maximum being independent of the wave period. A counter-argument is that this is potentially far too complex a picture and that simply waiting for a “calm” day is a more likely strategy for success. However, “calm” is only relative as even waves of quite small amplitude significant water displacements relative to the propagule scale.

5.5. Species-dependent advantages

Considering the species listed in Section 4.1, there is a factor of three variability in scale, around a factor of 50 in terms of density relative to seawater and around a factor of 2.5 variability in observed sinking rates. *Cystophora* and *Durvillaea* take opposing pathways

towards generating a sinking speed, with the former being relatively light but big whereas the latter is small and heavy. As a consequence of being related to scale, the Re_{sp} is not substantially different across species (a factor of three). Hence, Re_{sp} relates more to the physical situation that propagules find themselves in. This makes sense as in a parameter combining the flow characteristics with the particle scale.

Consequently, the scaling indicates that the most substantial difference in the propagule mechanics is that associated with its buoyancy. Fig. 10 shows BTR contours (BTR=20) for each species superimposed upon the most common wave conditions. At any point in the wave domain there is around two orders of magnitude variation in BTR across the three species. Similarly, there are significant differences in success between species (Taylor and Schiel, 2003), with *Hormosira* being the least successful at least for short times. Note however, the significant difference in timescales being considered — the ecological studies of Taylor and Schiel considered periods of over 1, 6 and 12 h, but the timescales here are wave and wave-group timescales (i.e. between 10 and 200 s).

The BTR scaling suggests buoyancy dominates for all species and also that it creates major species-differences. However, this simple viewpoint is complicated by a lack of knowledge about the mucous sheath and the actual time-varying packaging of propagules. Inclusion of the mucous effect suggests that differences among species in mucous coatings and buoyancy must have a considerable effect on reaching the substrate. Possibly of greater importance is the ability for buoyant propagule assemblages to remain in the “viable” part of the water column for as long as possible (e.g., not sinking out beneath the reef system to a sandy substrate), perhaps even enhancing aggregation. In addition, this might aid propagules settling on substrates that are near-vertical or even overhanging. The parameterization suggests that mucous-modified buoyancy may be very important (but with no method of measurement yet devised to support this conjecture).

This study did not address “attachment”, the next phase in the life-history of successful organisms in rocky systems. From a physics-only perspective we identify here that “high energy” clearly has some advantages for settlement. Yet *staying* settled (i.e., attachment) is probably best achieved in low-energy environments. At this point many and varied biochemical factors as well as physical influences come into play. Much of the scaling (e.g. SR) will also be relevant to quantification of likelihood of staying attached (Schiel et al., manuscript in prep.). Ecological studies

such as Taylor and Schiel (2003) observe settlement and attachment combined. Furthermore, neither the present study, nor that of Taylor and Schiel, addressed the actual released concentrations and distribution of propagules in the water column. It is likely that a very “unsteady” perspective must be taken, along the lines of combining Fig. 7 with biochemical evolution.

Acknowledgements

John McGregor, Iain MacDonald, Jack van Berkel and Spencer Wood assisted in the field. David Plew, Robyn Dunmore and Stéphane Popinet commented on aspects of the research. Richard Gorman kindly provided the wave hindcast data. An anonymous Reviewer is thanked for constructive comments especially relating to interpretation of the parameter domain figures. We gratefully acknowledge funding from the New Zealand Foundation for Research Science and Technology (Contracts C01X0501 and C01X0024) and the New Zealand Royal Society Marsden Fund (03-UOC-039).

References

- Abelson, A., Denny, M., 1997. Settlement of marine organisms in flow. *Ann. Rev. Ecol. Syst.* 28, 317–339. doi:10.1146/annurev.ecolsys.28.1.317.
- Baird, M.E., Atkinson, M.J., 1997. Measurement and prediction of mass transfer to experimental coral reef communities. *Limnol. Oceanogr.* 42, 1685–1693.
- Berndt, M.L., Callow, J.A., Brawley, S.H., 2002. Gamete concentrations and timing and success of fertilization in a rocky shore seaweed. *Mar. Ecol., Prog. Ser.* 226, 273–285.
- Burdick, G.M., Berman, N.S., Beaudoin, S.P., 2001. Describing hydrodynamic particle removal from surfaces using the particle Reynolds number. *J. Nanopart. Res.* 3, 455–467.
- Chiswell, S., Schiel, D.R., 2001. Influence of along-shore advection and upwelling on coastal temperature at Kaikoura Peninsula, New Zealand. *N.Z. J. Mar. Freshw. Res.* 35, 307–318.
- Clarke, S.M., Womersley, H.B.S., 1981. Cross-fertilization and hybrid development of forms of the brown alga *Hormosira banksii* (Turner) Decaisne. *Aust. J. Bot.* 29, 497–505.
- Clayton, M.N., 1992. Propagules of marine macroalgae: structure and development. *Br. Phycol. J.* 27, 219–232.
- Coon, D., Neushul, M., Charters, A.C., 1972. The settling behavior of marine algal spores. *Proc. Int. Seaweed Symp.* 7, 237–242.
- Crimaldi, J.P., Thompson, J.K., Rosman, J.H., Lowe, R.J., Koseff, J.R., 2002. Hydrodynamics of larval settlement: the influence of turbulent stress events at potential recruitment sites. *Limnol. Oceanogr.* 47, 1137–1151.
- Dade, W.B., 1993. Near-bed turbulence and the hydrodynamic control of diffusional mass transfer at the sea floor. *Limnol. Oceanogr.* 38, 52–69.
- Denny, M.W., Dairiki, J., Destefano, S., 1992. Biological consequences of topography on wave-swept rocky shores: I. enhancement of external fertilization. *Biol. Bull.* 183, 220–232.

- Dunmore, R.A., Schiel, D.R., 2003. Demography, competitive interactions and grazing effects of intertidal limpets in southern New Zealand. *J. Exp. Mar. Biol. Ecol.* 288, 17–38.
- Eckman, J.E., 1996. Closing the larval loop: linking larval ecology to the population dynamics of benthic invertebrates. *J. Exp. Mar. Biol. Ecol.* 200, 207–237.
- Emery, W.J., Thomson, R.E., 1997. *Data Analysis Methods in Physical Oceanography*. Pergamon, New York, p. 634.
- Fedderson, F., Gallagher, E.L., Guza, R.T., Elgar, S., 2003. The drag coefficient, bottom roughness, and wave-breaking in the nearshore. *Coast. Eng.* 48, 189–195.
- Friedlander, S.K., Johnstone, H.F., 1957. Deposition of suspended particles from turbulent gas stream. *Ind. Eng. Chem.* 49, 1151–1156.
- Gaylord, B.P., 1999. Detailing agents of physical disturbance: wave-induced velocities and accelerations on a rocky shore. *J. Exp. Mar. Biol. Ecol.* 239, 85–124.
- Gaylord, B., Reed, D.C., Raimondi, P.T., Washburn, L., McLean, S.R., 2002. A physically based model of macroalgal spore dispersal in the wave and current-dominated nearshore. *Ecology* 83, 1239–1251.
- Gorman, R.M., Bryan, K.R., Laing, A.K., 2003. Wave hindcast for the New Zealand region: nearshore validation and coastal wave climate. *N.Z. J. Mar. Freshw. Res.* 37, 567–588.
- Grant, W.D., Madsen, O.S., 1986. The continental-shelf bottom boundary layer. *Annu. Rev. Fluid Mech.* 18, 265–305. doi:10.1146/annurev.fl.18.010186.001405.
- Hay, C.H., 1994. *Durvillaea* (Bory). In: Akatsuka, I. (Ed.), *Biology of Economic Algae*. SPB Academic Publishers, The Netherlands, pp. 353–384.
- Hurd, C.L., 2000. Water motion, marine macroalgal physiology, and production. *J. Phycol.* 36, 453–472.
- Jorgensen, B.B., Revsbech, N.P., 1985. Diffusive boundary layers and the oxygen uptake of sediments and detritus. *Limnol. Oceanogr.* 30, 111–122.
- Kim, S.-C., Friedrichs, C.T., Maa, J.P.-Y., Wright, L.D., 2000. Estimating bottom stress in tidal boundary layer from acoustic Doppler velocimeter data. *J. Hydrol. Eng.* 126, 399–406.
- Koehl, M.A.R., Hadfield, M.G., 2004. Soluble settlement cue in slowly-moving water within coral reefs induces larval adhesion to surfaces. *J. Mar. Syst.* 49, 75–88.
- McGregor, J.A., Poulter, E.M., Smith, M.J., 1998. S-band radar measurements of wave energy fluxes and dissipation across an offshore bar. *J. Geophys. Res.* 103 (C9), 18,779–18,789.
- Nokes, R.I., 2005. *FluidStream v6.01: User's Guide*. Software Manual. University of Canterbury Christchurch, New Zealand.
- Norton, T.A., 1992. Dispersal by macroalgae. *Br. Phycol. J.* 27, 293–301.
- Puleo, J.A., Holland, K.T., 2001. Estimating swash zone friction coefficients on a sandy beach. *Coast. Eng.* 43, 25–40.
- Reidenbach, M.A., Monismith, S.G., Koseff, J.R., Yahel, G., Genin, A., 2006. Boundary layer turbulence and flow structure over a fringing coral reef. *Limnol. Oceanogr.* 51 (5), 1956–1968.
- Schiel, D.R., 2004. The structure and replenishment of rocky shore intertidal communities and biogeographic comparisons. *J. Exp. Mar. Biol. Ecol.* 300 (1–2), 309–342.
- Schiel, D.R., 2006. Rivets or bolts? When single species count in the function of temperate rocky reef communities. *J. Exp. Mar. Biol. Ecol.* 338, 233–252.
- Schiel, D.R., Foster, M.S., 2006. The population biology of large brown seaweeds: consequences of multi-phase life histories in dynamic coastal environments. *Ann. Rev. Ecol. Syst.* 37, 343–372.
- Schlichting, H., 1979. *Boundary-Layer Theory*, 7th ed. McGraw Hill, New York.
- Shimeta, J., 1993. Diffusional encounter of submicrometer particles and small cells by suspension feeders. *Limnol. Oceanogr.* 38, 456–465.
- Shimeta, J., Jumars, P.A., 1991. Physical mechanisms and rates of particle capture by suspension feeders. *Oceanogr. Mar. Biol. Ann. Rev.* 29, 191–257.
- Taylor, D.I., Schiel, D.R., 2003. Wave-related mortality in propagules of habitat-forming algae from different exposures in southern New Zealand: the importance of “stickability”. *J. Exp. Mar. Biol. Ecol.* 290, 229–245.
- Taylor, D., Delaux, S., Schiel, D., Stevens, C., Nokes, R., 2008. Attachment of fucoid species under the influence of turbulence.
- Tritton, D.J., 1988. *Physical Fluid Dynamics*, 2nd Ed. Oxford Univ. Press, Oxford pp. 536.
- Young, I., 1999. *Wind Generated Ocean waves*. Elsevier, Oxford, pp. 288.